PROCEEDINGS A

royalsocietypublishing.org/journal/rspa

Research

Cite this article: Butler PA. 2023 Enhancing the performance of solenoidal spectrometers for inverse reactions. *Proc. R. Soc. A* **479**: 20230075.
https://doi.org/10.1098/rspa.2023.0075

Received: 1 February 2023
Accepted: 2 May 2023

Subject Areas:
nuclear physics

Keywords:
nuclear instrumentation, charged-particle spectrometer, transfer reactions, inelastic scattering, radioactive beams

Author for correspondence:
P. A. Butler
e-mail: peter.butler@liverpool.ac.uk

Enhancing the performance of solenoidal spectrometers for inverse reactions

P. A. Butler

Oliver Lodge Laboratory, University of Liverpool, Liverpool L69 7ZE, UK

PAB, 0000-0001-6080-9205

Helical-orbit solenoidal spectrometers, in which the target and detector are placed inside a uniform magnetic field, have been utilized for more than a decade to study nuclear reactions in inverse kinematics, induced by radioactive beams. Methods to improve the final-state energy resolution are presented, and the inclusion of an active gas target is proposed to improve the performance of the spectrometer.

1. Introduction

To understand the underlying quantum structure of atomic nuclei, measurements that use reactions to probe nuclear properties should be carried out with a precision that is sensitive to this structure. Transfer reactions such as (d,p) and inelastic scattering reactions such as (d,d′) have been employed for many decades to make direct measurements of the single-particle and collective properties of nuclear states. For reactions induced by intense beams of light ions bombarding stable targets, final-state energy resolutions of ≈10 keV can be achieved using magnetic spectrographs, see, e.g. [1,2]. To study nuclei beyond the line of stability, the detector system, whose precision is determined by the detector design, the target and the characteristics of the beam, has to be highly efficient to exploit the much weaker flux of radioactive beams [3]. In this case, the states of interest are populated by an inverse reaction, usually by bombarding a solid deuterated polyethylene $[(C_2D_4)_n]$ target. This would normally have the disadvantage that the strong dependence of the energies of the emitted light

THE ROYAL SOCIETY PUBLISHING

ions on their angle of emission will lead to kinematic broadening, and the separation between the laboratory energies of the excited states will be highly compressed.

These difficulties have largely been overcome by employing an ingenious technique, developed at the Argonne National Laboratory, whereby the emitted light particles are transported in a homogeneous magnetic field $\boldsymbol{B}$, parallel to the beam axis, to a position-sensitive silicon detector array [4,5]. Here, both the particle energy and the distance between the target and the intercept of the particle's trajectory with the beam axis are recorded to determine the excitation energy of the state of interest, which has a linear dependence on these quantities (see §2). This spectrometer allows the angular distribution of the emitted particles to be measured with high efficiency over a wide angular range. In addition, the value of the ratio of mass-to-charge of the particle can be determined from the time of flight, which is the cyclotron period for the particle motion in a magnetic field. The spectrometer employing this concept is called the helical orbit spectrometer (HELIOS) and has been used successfully for over a decade at the ANL ATLAS facility. More recently, the ISOLDE Solenoidal Spectrometer (ISS), using the same principle of operation, has also been in operation employing radioactive beams from the HIE-ISOLDE facility, CERN, and the Solenoidal Spectrometer Apparatus for Reaction Studies (SOLARIS) [6], has been constructed to take beams from the FRIB facility in the Michigan State University campus.

This article presents some ideas for improving the response of spectrometers using the HELIOS concept. In §2, the various contributions to the total energy resolution of the excited states are estimated, and suggestions for reducing some of these contributions are presented. Section 3 presents a proposal to replace the solid target by an extended gas volume, where the reaction vertex is determined using a time-projection chamber.

2. Contributions to energy resolution

We consider the two-body reaction $M_1 + M_2 \rightarrow M_3 + M_4$, where M_1 is the mass of the (heavy) projectile and M_2 is the mass of the (light) target. For the spectrometer using the HELIOS concept, the light ejectile, having a charge state q and mass M_4, is emitted at the origin where the reaction occurs, the vertex. The particle, having energy E_4 in the laboratory frame of reference, travels in a magnetic field with flux density $\boldsymbol{B}$, which is parallel to the beam axis until its trajectory intercepts with the beam axis at distance z from the origin. In this case, the energy of the excited state of the residual nucleus of mass M_3 can be determined from the reaction Q-value, which is a linear function of E_4 and z:

$$Q = aE_4 + b - cz, \tag{2.1}$$

where a, b and c are constants given by

$$a = \frac{(M_3 + M_4)}{M_3}$$

$$b = \frac{aM_4 v_{\mathrm{cm}}^2}{2} - \frac{M_2 E_0}{(M_1 + M_2)}$$

and

$$c = \frac{aM_4 v_{\mathrm{cm}}}{T_{\mathrm{cyc}}}.$$

In the aforementioned expressions, E_0 is the beam energy, v_{cm} is the velocity of the centre-of-mass system,

$$v_{\mathrm{cm}} = \frac{\sqrt{2M_1 E_0}}{(M_1 + M_2)},$$

and T_{cyc} is the cyclotron period of the light particle in the magnetic field,

$$T_{\mathrm{cyc}} = \frac{2\pi M_4}{(qeB)}.$$

In the case of inelastic scattering reactions for which $M_2 = M_4$, $b = 0$.

To determine the various contributions to the spread in the measured values of Q, the reaction and trajectory from the target to the detector can be simulated under differing conditions. In this Monte Carlo simulation [7], the centre-of-mass scattering angle was stepped over in 0.2° increments and 100 passes made for each angle. For each pass, the beam trajectory, ejectile trajectory and detector response were calculated assuming random (usually Gaussian) distributions of position, angle, energy, etc.; the ejectile trajectory was calculated by integrating the equations of motion in the magnetic and electric fields using a step time of 1ps. The incident beam will have a divergence and finite size at the target, as well as a spread in energy. Both the heavy beam and the emitted light particle will suffer energy loss, energy straggling and multiple scattering in the target. In the passage to the detector, the magnetic field will not be perfectly homogeneous. When the light particle reaches the silicon detector, there will be an uncertainty in the measured value of z, the distance between the intercept of its trajectory on the beam axis and the target. These simulations modelled the response of the Si array for the ISS, which has the shape of a hexagonal prism in which each of the six rectangular faces is parallel to the beam direction and consists of four 22 mm × 125 mm double-sided silicon detectors. The perpendicular distance from the face of each detector to the beam axis is ≈29 mm so that the detectors subtend ≈70% of 2π in the plane transverse to this axis. The Si detectors are segmented along the z-direction to give z_{Si} and along the transverse direction, enabling the radius of the trajectory at the intercept r_{Si} to be determined. As the Si array is at a finite radius from the beam axis, these values are used to extrapolate the particle's trajectory to the beam axis. The quantities z, r, z_{Si} and r_{Si} are defined in the appendix that outlines a simple algorithm that can be used to determine z from z_{Si} and r_{Si}. The finite pitch of the segmentation will give rise to an uncertainty in the value of z and hence the Q-value. Finally, the intrinsic energy resolution of the Si array will also contribute to the uncertainty in the Q-value. For a typical case, the Q-value, calculated from the values of z and E_4 determined for each event, was sampled several thousand times, allowing its variance to be estimated.

The parameters used in the simulations are given in table 1. The energy loss and energy straggling of the beam and light ions in the target were calculated using the SRIM codes [8]. The angular dependence of the multiple scattering was assumed to have a Gaussian distribution whose width was calculated using the Fano prescription described by Kantele [9]. For traversing through gas (see §3), the value of the width was reduced to empirically reproduce the measurements of Kuhn *et al.* [10]. Figure 1 shows the contributions to the expected Q-value resolution for the inverse reaction ^{206}Hg(d,p)^{207}Hg at a bombarding energy of 7.38 MeV u^{-1}. The nominal Q-value for the reaction was set to zero. Figure 1(*a*) assumes that the uncertainties are given by set 1 in table 1 that are the typical values for HELIOS spectrometers. The full width at half maximum (FWHM) Q-value resolution actually measured using the HELIOS Si array, 165 µg cm^{-2} $(C_2D_4)_n$ target and a ^{206}Hg beam from the HIE-ISOLDE post-accelerator was 140 keV [11]. (The characteristics of the Si array used in this experiment are given in [5] and differ slightly from those given in set 1). Figure 1(*b*) assumes the values given in set 2, where the intrinsic energy resolution is reduced from 50keV to 10keV FWHM and the target thickness is reduced from 165 to 10 µg cm^{-2}. This improves the overall Q-value resolution from ≈160 to ≈45 keV FWHM. The loss in luminosity can be regained to some extent by employing multiple targets, spaced apart sufficiently to identify the reaction vertex by measuring the heavy recoil's time of flight to a detector placed downstream. An intrinsic Si energy resolution of 10 keV FWHM or better resolution should be achievable for proton detection [12]; however, for the complex Si arrays used in the HELIOS setup, the best resolution achieved at present is 25 keV FWHM [5]. As shown in figure 1, significant contributions to the overall Q-value resolution come from the beam characteristics, in this case being typical values for HIE-ISOLDE [13]. The transverse emittance of the beam, which determines the beam divergence and the size of the beam spot, can be reduced by collimation, while the energy spread can be reduced by operating a Linac cavity of the post-accelerator as a buncher [14]. Such improvements in the beam characteristics can also be achieved by injection into, and extraction from, a storage ring that cools the circulating beam [15]. The values given in set 3 can be obtained for optimized beams from HIE-ISOLDE. The contributions

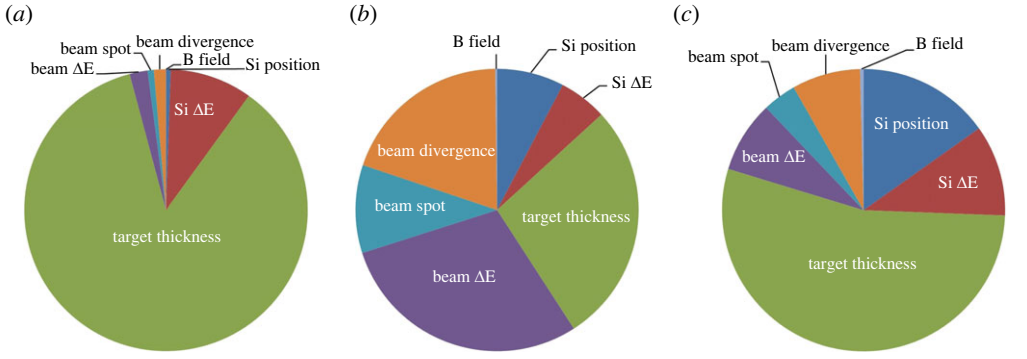

Figure 1. The contributions to the total *Q*-value resolution of the ISOLDE Solenoidal Spectrometer for differing conditions. (*a*) It is assumed that the uncertainties are given by set 1 in table 1 that are the typical values for HELIOS spectrometers. (*b*) The intrinsic energy resolution is reduced from 50 keV to 10 keV FWHM, and the target thickness is reduced from 165 to 10 μg cm^{-2}. (*c*) The beam characteristics are optimized by reducing the transverse emittance and energy spread. The area of each sector is proportional to the square of the *Q*-value resolution arising from the contribution alone.

Table 1. The various contributions to the uncertainty in the value of *Q*. All uncertainties are FWHM except for the detector pitch and target thickness.

source of uncertainty	set 1	set 2	set 3
Si pitch *z*-direction (mm)	0.95	0.95	0.95
Si pitch transverse direction (mm)	2	2	2
detector *E* resolution (keV)	50	10	10
target thickness (mg cm^{-2})	0.165	0.010	0.010
beam *E* spread (%)	0.4	0.4	0.15
beam spot (mm)	2.3	2.3	1.0
beam divergence (mrad)	1.8	1.8	0.8
B variation (%)	0.5	0.5	0.5
overall *Q*-value resolution (keV)	160	45	30

to the *Q*-value resolution, ≈30 keV FWHM overall, are shown in figure 1. However, to reduce the transverse emittance to a value that gives the tabulated beam characteristics, the beam intensity will be reduced to ≈25% of its initial value. The reduction in beam intensity and target thickness would prohibit the use of radioactive beams in many cases.

3. Adoption of gas active target, HELIOS-TPC

In this mode of operation, the target is now a gas, e.g. deuterium, in a homogeneous electric field ***E***, parallel to ***B***. This combines the HELIOS concept with that of the time-charge projection chamber (TPC), the latter employed successfully in low-energy nuclear physics applications for two decades (see, e.g. [16,17]) and more recently operating inside a solenoidal magnetic field [18,19]. For recent reviews of active targets, see [20,21]. In an active target, pure gases such as H_2, D_2 and N_2 can be employed, for which there will be almost no background from carbon-induced events. For ^{3,4}He, a small amount (5%) of N_2 or CO_2 is added. For rare, radioactive isotopes such as tritium, self-contained and sealed cells can be used to reduce the activity from the gas volume, as suggested in [22]. The proposed layout of the hybrid spectrometer is shown

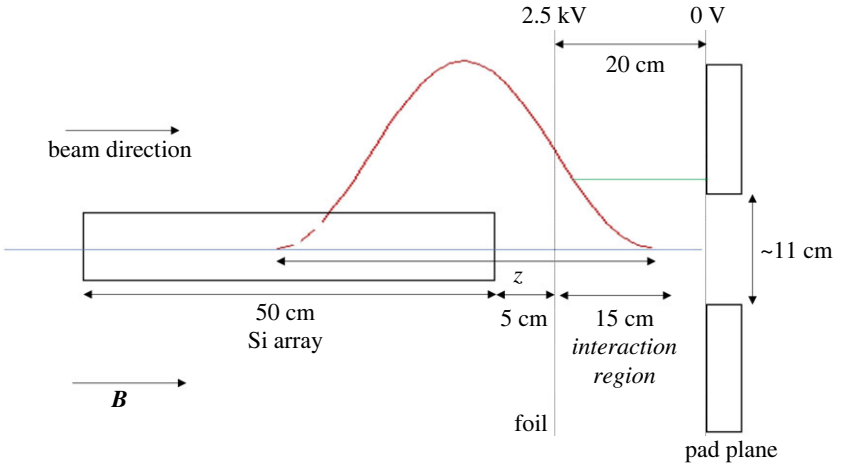

Figure 2. Layout of the hybrid detector, HELIOS-TPC. The $\boldsymbol{E}$ field is parallel to the $\boldsymbol{B}$ field and the beam direction. The interaction region is 15 cm in the z-direction.

in figure 2. Here, the high voltage plane lies close to the Si array, and the ionization charges in the gas produced by the passage of the light ejectile through the gas are collected in the sensor plane that is placed downstream of the interaction region. For each event, the values of z_p and r_p (see appendix) are determined from the drift time and position of the collected charges on the sensor plane. The z-position of the reaction vertex can then be deduced by extrapolation using the algorithm described in the appendix. The sensor plane is typically equipped with a Micromegas device [23], consisting of a printed circuit board covered with electrodes, or *pads*. The charge drift velocity in the arrangement shown in figure 2 will give a maximum collection time of $\approx 10\,\mu s$ for a pressure of 50 Torr D_2. The reaction zone and the immediate surrounding volume are shielded from the time-projection pads. This ensures that the beam particles and small angle elastic scattering events are not detected, important to maximize the luminosity of the experiment (see later). Similar considerations led to the design of the TACTIC [24] and ANASEN [25] active-target detectors. To investigate the performance of this hybrid spectrometer, simulations were carried out assuming the same silicon array as described in §2 and 3 mm time-projection pads at a radius of 5.5 cm. The z-position of the reaction vertex can then be deduced by extrapolation using the algorithm described in the appendix. For reactions such as (d,p) or (α,p), where protons emitted backwards are detected, events arising from elastic scattering can be easily rejected. For forward-going reactions such as (d,d'), the pads are placed upstream of the target region. In this case, the reaction vertex, pad and Si detector define the cyclotron trajectory in the x–y plane, which is then matched to that calculated from E_4 and z. The perturbation of this trajectory due to energy loss in deuterium or helium gas is very small and can be corrected.

In table 2, the maximum luminosity L_{max}, defined numerically as the product of the maximum beam intensity I (ions s^{-1}), the target thickness t (mg cm^{-2}) and the absolute efficiency of the detector system ϵ are estimated for the hybrid spectrometer and compared with experimental measurements using radioactive beams. The measurements used the active-target spectrometer AT-TPC with 600 Torr He (with 5% CO_2) to study the reaction $^{22}Mg(\alpha,p)^{25}Al$ [26] or ISS with $(C_2D_4)_n$ targets to study $^{28}Mg(d,p)^{29}Mg$ [27] and $^{206}Hg(d,p)^{207}Hg$ [11]. For the hybrid system, the beam interaction region is assumed to be 15 cm of 50 Torr He or 50 Torr D_2. The latter is equivalent to 0.67 mg cm^{-2} $(C_2D_4)_n$. An important consideration in determining L_{max} is the rate of elastically scattered target recoils that can potentially give a high instantaneous rate in the pad detectors, limiting the maximum beam intensity. In the case of HIE-ISOLDE, the magnesium beam intensities given in table 2 for the simulations are limited by the capability of the ISOLDE

Table 2. Maximum luminosities and widths of Q-value distribution estimated for various reactions from the simulations of the performance of the HELIOS-TPC hybrid detector with 50 Torr gas. These are compared with the actual luminosities achieved for the experiments (see the text) and experimental measurements of the Q-value resolution. For the simulations, the nominal value of the reaction Q was zero. For the experiments using $(C_2D_4)_n$ targets, the total target thickness is given.

	hybrid HELIOS-TPC (simulation)				AT-TPC or ISS (see text)				
reaction	beam energy MeV u^{-1}	beam intensity ions s^{-1}	luminosity L_{max} $I \cdot t \cdot \epsilon$	Q-value FWHM keV	beam intensity ions/s	target thickness mg cm^{-2}	luminosity L_{max} $I \cdot t \cdot \epsilon$	Q-value FWHM keV	reference
^{22}Mg(α,p)	5	6×10^5	6×10^4	93	900	13	6.5×10^3	≈300	[26]
^{28}Mg(d,p)	9.47	10^6	9.7×10^4	75	10^6	0.12	1.8×10^4	130	[27]
^{206}Hg(d,p)	7.38	1.5×10^5	1.3×10^4	70	5×10^5	0.17	1.2×10^4	140	[11]
^{86}Kr(d,p)	10	2.5×10^6	2.7×10^5	75	5×10^7	0.06	4.3×10^5	80	[28]
^{136}Xe(d,p)	10	5×10^5	5×10^4	75	5×10^6	0.15	1.3×10^5	100	[29]

primary target ion source. For the ^{206}Hg beam intensity given in the table, the average rate of scattered target recoils is 10^3/s integrated over all angles for which the trajectory of the ion in the magnetic field, moderated by energy loss in the gas, reaches further than 5.5 cm from the beam axis. The macroscopic beam structure of the HIE-ISOLDE linear accelerator has ≈1 ms pulses with a repetition rate determined by the charge breeding time in the EBIS ion source. For mass ≈200 ions, this is ≈200 ms [13], giving an instantaneous rate of ≈200 per beam pulse, i.e. two events in the 10 µs collection time. While this is approaching the limit for the sampling electronics for a full tracking active-target spectrometer such as the AT-TPC [18,20], the simplified pad array envisaged here should be able to accept a higher event rate.

The angular-dependent efficiency of the hybrid system that takes into account the electric field cage surrounding the active-target region is shown in figure 3 for four reactions listed in table 2 and compared with the simulated efficiency of HELIOS employing a $(C_2D_4)_n$ target or the measured AT-TPC efficiency [26]. The cutoff at low values of θ_{cm} (high values of ζ_{lab}) is determined by the chosen energy threshold for detection of protons in the Si array. The highest value of θ_{cm} detected is limited either by the closest distance of the interaction region to the Si array or by the finite radius of the magnet. The overall efficiency is 50–60%, comparable to that of the ISS and that of the AT-TPC. Table 2 demonstrates that the maximum luminosity for the hybrid spectrometer compares favourably with both active target and HELIOS spectrometers. Also included in table 2 are the luminosities estimated for the ^{86}Kr(d,p)^{87}Kr and ^{136}Xe(d,p)^{137}Xe stable-beam reactions. These reactions were studied using HELIOS at the ATLAS facility [28,29] where the intensity of the beam, produced by an ECR source with 100% duty factor, was limited to prevent damage of the targets. For the hybrid spectrometer, it was assumed that the beam intensity is limited by the instantaneous count rate arising from the poor duty factor of the HIE-ISOLDE linac. In this case, the luminosity for the hybrid device is within a factor of two of that achieved using HELIOS.

Another advantage of employing an active gas target is that the energy loss of the beam in the target and the energy loss of the ejectile in the gas volume and any foils (typically 100 keV or less) can be determined reasonably accurately for each event. This means that the only contribution from the gas to the overall energy resolution arises from multiple scattering and straggling. For a pressure of 50 Torr gas, the total FWHM Q-value resolution is estimated for the five reactions listed in table 2. In these simulations, it is assumed that the FWHM uncertainty in the z-position of the ejectile trajectory in the gas from the charge collection time is 1 mm. The goal of achieving this position resolution will determine the design of the pad structure. In addition, beam energy loss, straggling and multiple scattering in the gas entrance window (assumed to be 100 µg cm^{-2}

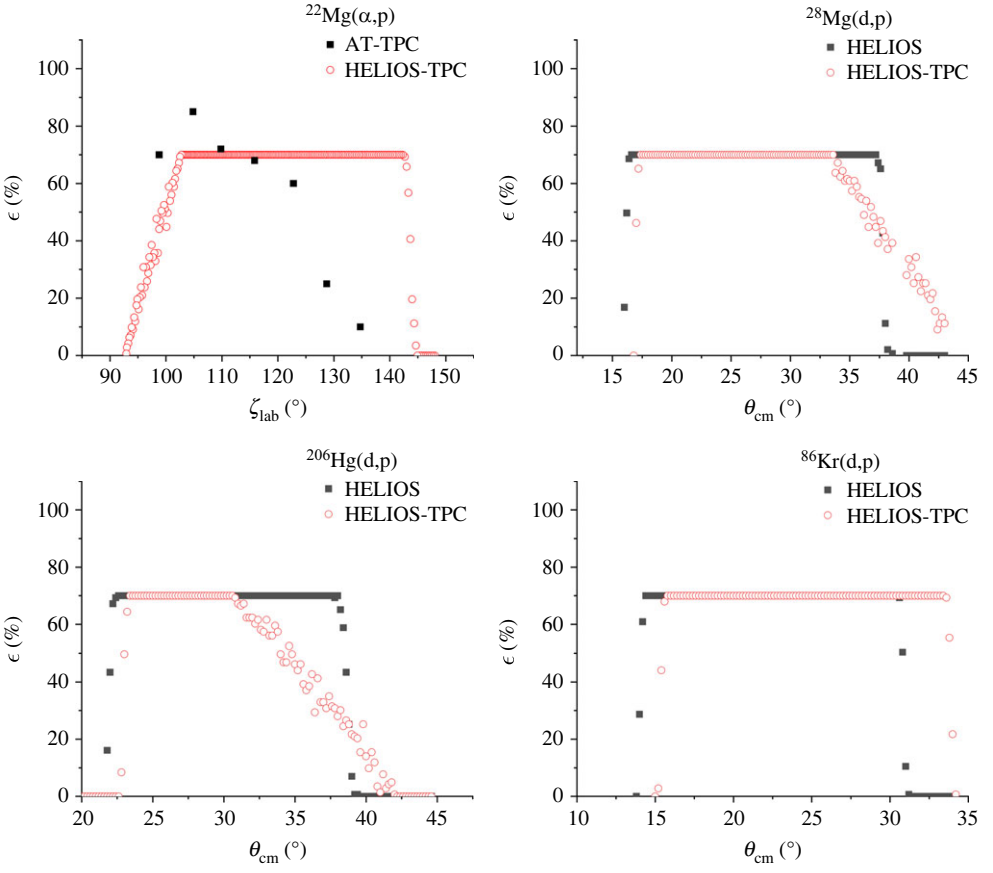

Figure 3. Efficiency, ϵ, for detection of protons in the silicon array from four reactions listed in table 2 as a function of the laboratory scattering angle of the ejectile ζ_{lab} or centre-of-mass scattering angle θ_{cm}. For the ^{22}Mg(α,p)^{25}Al reaction the black solid squares are measured values for the AT-TPC [26]. For the (d,p) reactions the black solid squares are values from the simulations described in the text for the HELIOS-like spectrometer ISS. The red open circles are for the hybrid HELIOS-TPC spectrometer assuming the layout of figure 2 with 50Torr He or D_2 gas. The simulations use a nominal value for the reaction Q of zero.

polypropylene) and the path to the interaction region were taken into account. The characteristics of the Si detector array, the beam and the magnetic field were assumed to be the same as those listed in set 1 in table 1. The energy loss of the ejectiles in the foil that provides the equipotential plane near the Si array, assumed to be metal-coated 50 μg cm^{-2} polypropylene, was ignored: for 5 MeV protons, the energy loss in such a foil is $\approx$5 keV that can be estimated for each event. The values of the Q-value resolution determined from the simulations are given table 2. In the case of the radioactive beam reactions, these values are significantly smaller than those measured for the active target spectrometer [26] or the ISS spectrometer [11,27]. For the stable beam reactions ^{86}Kr(d,p) and ^{136}Xe(d,p), the Q-value resolution was estimated to be 75keV for the hybrid spectrometer. This can be compared to the 80 keV value measured for the former reaction using HELIOS with a 60 μg cm^{-2} target [28] and 100 keV for the latter reaction using a 150 μg cm^{-2} target [29]. However, an improved energy resolution can be achieved if the gas pressure is reduced: for a D_2 pressure of 10 Torr and intrinsic Si energy resolution of 20 keV, the Q-value resolution is estimated to be 45 keV for the ^{206}Hg(d,p)^{207}Hg reaction and 55 keV for the ^{86}Kr(d,p)^{87}Kr and ^{136}Xe(d,p)^{137}Xe reactions. In this case, the maximum luminosity is reduced by between a third and a half, and remains comparable to that measured using the HELIOS spectrometers.

4. Summary

The various contributions to the final-state, or Q-value energy resolution of a helical-orbit solenoidal spectrometer, have been considered. The largest contribution usually arises from effects of energy loss and multiple scattering in the target, with significant contributions from intrinsic energy resolution of the Si detector array and the characteristics of the beam. The Q-value energy resolution can be improved by reducing the target thickness and manipulating the beam, but the resulting large reduction in luminosity may not be desirable for studying reactions induced by low-intensity radioactive beams. It is proposed to replace the composite solid target by an extended gas volume, e.g. pure deuterium, so that the hybrid spectrometer combines the properties of the HELIOS spectrometer and that of a time-projection chamber. This will remove contributions from carbon-induced reactions involving hydrogen or deuterium targets and allow helium-induced reactions to be studied. It is shown that HELIOS-TPC will enable experiments to achieve good energy resolution without compromising the luminosity of the experiment.

Data accessibility. The software package supporting this article is published [7] under the GNU General Public License v. 3.0.

Authors' contributions. P.B.: conceptualization, data curation, formal analysis, funding acquisition, investigation, methodology, project administration, resources, software, supervision, validation, visualization, writing—original draft and writing—review and editing.

Conflict of interest declaration. I declare I have no competing interest.

Funding. This work was supported by the Science and Technology Facilities Council (UK) grant no. ST/V001027/1.

Acknowledgements. The author acknowledges useful discussions with Yassid Ayyad, Daniel Bazin, Andreas Ceulemans, Matthew Fraser, Sean Freeman, Liam Gaffney, Jack Henderson, Benjamin Kay, Marc Labiche, Alison Laird, Robert Page, Oleksii Poleshchuk, Riccardo Raabe, David Sharp and Fredrik Wenander.

Appendix A. Algorithm to extrapolate intersection of ejectile trajectory on beam axis

The following assumes an active target configuration as shown in figure 2, where the reaction vertex is determined using the time projection method. If a solid $(C_2D_4)_n$ target is employed, then only the second step is necessary, with $z_v = 0$.

First step. The value of z_v, the position of the reaction vertex, is extrapolated from z_p, the position of the ejectile trajectory measured at radius r_p using the pad detector. The value of r_p is related to the rotation of the cyclotron motion in the magnetic field, see figure 4, by

$$r' = r_p = \rho_{max} \sin\left(\frac{\alpha_p}{2}\right),$$

where

$$\rho_{max} = 2r = 2\frac{\sqrt{2E_4M_4}}{qeB}\sin\zeta \tag{A 1}$$

and

$$\cos\zeta = (z_i - z_v)/\frac{2\pi\sqrt{2E_4M_4}}{qeB}. \tag{A 2}$$

In these equations, ζ is the laboratory angle of emission of the ejectile, with respect to the beam axis and the direction of $\boldsymbol{B}$. The value of $z = z_i - z_v$ (z_i is the position of intersection on the beam axis after one cyclotron period) can be estimated using equation (2.1), since E_4 is measured. As $z_i - z_v \gg z_p - z_v$, a nominal value of Q can be used to make an initial estimate of z, and hence, α_p.

Now,

$$\frac{(z_p - z_v)}{(z_i - z_v)} = \frac{\alpha_p}{2\pi},$$

allowing z_v to be determined.

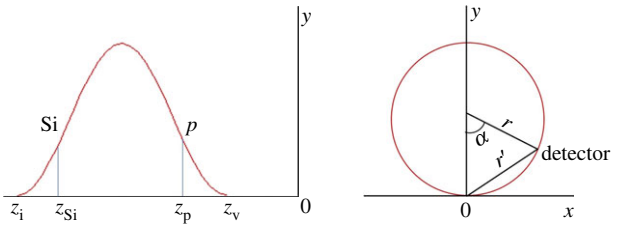

Figure 4. The projection of the trajectory of the light particle in the magnetic field in the $z - y$ and $x - y$ planes, showing its relation to the position of the intersection on the pad detector (z_p) and silicon detector (z_{Si}).

Second step. The value of z_i is estimated more accurately from z_{Si}, which is measured using the Si detector array. The procedure is the same as for step 1 except that the radial position at the Si detector (from the transverse displacement and detector geometry) is given by

$$r' = r_{Si} = \rho_{max} \sin\left(\frac{\alpha_{Si}}{2}\right).$$

The initial estimate of $(z_i - z_v)$ is $(z_{Si} - z_v)$, and ρ_{max} is determined using equations (A 1) and (A 2). In this case,

$$\frac{(z_i - z_{Si})}{(z_i - z_v)} = \frac{\alpha_{Si}}{2\pi},$$

from which a better estimate of z_i can be determined.

The whole procedure is repeated and rapidly converges, so that the value of z changes by less than 0.1 mm, typically after five iterations or less.

References

1. Von Egidy T *et al.* 1981 The rotational structure of ^{227}Ra. *Nucl. Phys. A* **365**, 26–60. (doi:10.1016/0375-9474(81)90386-9)
2. Thorsteinsen TF, Nybø K, Løvhøiden G. 1990 Levels in ^{226}Ra populated by inelastic deuteron scattering. *Phys. Scr.* **42**, 141–144. (doi:10.1088/0031-8949/42/2/004)
3. Wimmer K. 2018 Nucleon transfer reactions with radioactive beams. *J. Phys. G: Nucl. Part. Phys.* **45**, 033002. (doi:10.1088/1361-6471/aaa2bf)
4. Wuosmaa AH, Schiffer JP, Back BB, Lister CJ, Rehm KE. 2007 A solenoidal spectrometer for reactions in inverse kinematics. *Nucl. Instrum. Meth. A* **580**, 1290–1300. (doi:10.1016/j.nima.2007.07.029)
5. Lighthall JC *et al.* 2010 Commissioning of the HELIOS spectrometer. *Nucl. Instrum. Meth. A* **622**, 97–106. (doi:10.1016/j.nima.2010.06.220)
6. Kay BP, Hoffman CR, Wuosmaa AH. 2018 SOLARIS White Paper. See https://www.anl.gov/reference/solaris-white-paper.
7. Butler PA. 2023 *Helios simulation software*. See https://github.com/peterabutler/Helios.
8. Ziegler JF, Ziegler MD, Biersack JP. 2010 SRIM—the stopping and range of ions in matter. *Nucl. Instrum. Meth. B* **268**, 1818–1823. (doi:10.1016/j.nimb.2010.02.091)
9. Kantele J. 1995 *Handbook of nuclear spectrometry*. London: Academic Press.
10. Kuhn S, Eversheim PD, Hinterberger F, Von Rossen P, Trelle RP. 1984 Multiple scattering of protons in thick gas targets. *Nucl. Instrum Meth. B* **4**, 332–336. (doi:10.1016/0168-583X(84)90576-7)
11. Tang TL *et al.* 2020 First exploration of neutron shell structure below lead and beyond $N = 126$. *Phys. Rev. Lett.* **124**, 062502. (doi:10.1103/PhysRevLett.124.062502)
12. Steinbauer E, Bauer P, Geretschläger M, Bortels G, Biersack JP, Burger P. 1994 Energy resolution of silicon detectors: approaching the physical limit. *Nucl. Instrum Meth. B* **85**, 642–649. (doi:10.1016/0168-583X(94)95898-X)
13. Kadi Y, Blumenfeld Y, Delsolaro WV, Fraser MA, Huyse M, Koufidou AP, Rodriguez JA, Wenander F. 2017 Post-accelerated beams at ISOLDE. *J. Phys. G: Nucl. Part. Phys.* **44**, 084003. (doi:10.1088/1361-6471/aa78ca)

14. Lozano M, Bidault N, Fadakis E, Fraser MA, Matli E, Rodriguez JA. 2018 Characterization of the beam energy spread at the REX/HIE-ISOLDE Linac. *Proc. 9th Int. Particle Accelerator Conference, IPAC2018, Vancouver, 29 April – 4 May 2018*, pp. 787–789. Geneva: JACoW Publishing. (doi:10.18429/JACoW-IPAC2018-TUPAF042)
15. Butler PA *et al.* 2016 TSR: a storage and cooling ring for HIE-ISOLDE. *Nucl. Instrum Meth. A* **376**, 270–274. (doi:10.1016/j.nimb.2015.12.006)
16. Mizoi Y *et al.* 1999 Multiple-sampling and tracking proportional chamber for nuclear reactions with low-energy radioactive isotope beams. *Nucl. Instrum Meth. A* **431**, 112–122. (doi:10.1016/S0168-9002(99)00253-3)
17. Demonchy CE *et al.* 2007 MAYA, a gaseous active target. *Nucl. Instrum Meth. B* **573**, 145–148. (doi:10.1016/j.nima.2006.11.025)
18. Bradt J *et al.* 2017 Commissioning of the active-target time projection chamber. *Nucl. Instrum Meth. A* **875**, 65–79. (doi:10.1016/j.nima.2017.09.013)
19. Poleshchuk O, Raabe R, Ceruti S, Ceulemans A, De Witte H, Marchi T, Mentana A, Refsgaard J, Yang J. 2021 The SpecMAT active target. *Nucl. Instrum Meth. A* **1015**, 165765. (doi:10.1016/j.nima.2021.165765)
20. Beceiro-Novo S, Ahn T, Bazin D, Mittig W. 2015 Active targets for the study of nuclei far from stability. *Prog. Part. Nucl. Phys.* **84**, 124–165. (doi:10.1016/j.ppnp.2015.06.003)
21. Bazin D, Ahn T, Ayyad Y, Beceiro-Novo S, Macchiavelli AO, Mittig W, Randhawa JS. 2020 Low energy nuclear physics with active targets and time projection chambers. *Prog. Part. Nucl. Phys* **114**, 103790. (doi:10.1016/j.ppnp.2020.103790)
22. Ayyad Y *et al.* 2020 Next-generation experiments with the active target time projection chamber (AT-TPC). *Nucl. Instrum Meth. A* **954**, 161341. (doi:10.1016/j.nima.2018.10.019)
23. Giomataris Y, Rebourgeard P, Robert JP, Charpak G. 1996 MICROMEGAS: a high-granularity position-sensitive gaseous detector for high particle-flux environments. *Nucl. Instrum Meth. A* **376**, 29–35. (doi:10.1016/0168-9002(96)00175-1)
24. Fox SP *et al.* 2011 TACTIC: a new detector for nuclear astrophysics experiments. *J. Phys: Conf. Ser.* **312**, 052007. (doi:10.1088/1742-6596/312/5/052007)
25. Koshchiy E *et al.* 2017 ANASEN: the array for nuclear astrophysics and structure with exotic nuclei. *Nucl. Instrum Meth. A* **870**, 1–11. (doi:10.1016/j.nima.2017.07.030)
26. Randhawa JS *et al.* 2020 First direct measurement of ^{22}Mg(α,p)^{25}Al and implications for X-ray burst model-observation comparisons. *Phy. Rev. Lett.* **125**, 202701. (doi:10.1103/PhysRevLett.125.202701)
27. MacGregor PT *et al.* 2021 Evolution of single-particle structure near the $N = 20$ island of inversion. *Phys. Rev. C* **104**, L051301. (doi:10.1103/PhysRevC.104.L051301)
28. Sharp DK *et al.* 2013 Neutron single-particle strength outside the $N = 50$ core. *Phys. Rev. C* **87**, 014312. (doi:10.1103/PhysRevC.87.014312)
29. Kay BP *et al.* 2011 Single-neutron energies outside ^{136}Xe. *Phys. Rev. C* **84**, 024325. (doi:10.1103/PhysRevC.84.024325)